Emptying of Large-Scale Pipeline by Pressurized Air

Janek Laanearu, Ph.D.[1]; Ivar Annus, Ph.D.[2]; Tiit Koppel, Ph.D.[3]; Anton Bergant, Ph.D.[4]; Sašo Vučković[5]; Qingzhi Hou, Ph.D.[6]; Arris S. Tijsseling, Ph.D.[7]; Alexander Anderson, Ph.D.[8]; and Jos M. C. van't Westende, Ph.D.[9]

Abstract: Emptying of an initially water-filled horizontal PVC pipeline driven by different upstream compressed air pressures and with different outflow restriction conditions, with motion of an air-water front through the pressurized pipeline, is investigated experimentally. Simple numerical modeling is used to interpret the results, especially the observed additional shortening of the moving full water column due to formation of a stratified water-air "tail." Measured discharges, water-level changes, and pressure variations along the pipeline during emptying are compared using control volume (CV) model results. The CV model solutions for a nonstratified case are shown to be delayed as compared with the actual measured changes of flow rate, pressure, and water level. But by considering water-column mass loss due to the water-air tail and residual motion, the calibrated CV model yields solutions that are qualitatively in good agreement with the experimental results. A key interpretation is that the long air-cavity celerity is close to its critical value at the instant of minimum flow acceleration. The influences of driving pressure, inertia, and friction predominate, with the observed water hammer caused by the initiating downstream valve opening insignificantly influencing the water-air front propagation. **DOI: 10.1061/(ASCE)HY.1943-7900.0000631.**

CE Database subject headings: Air-water interactions; Drainage; Experimentation; Pipes; Pipelines; Transient flow; Unsteady flow.

Author keywords: Air-water interactions; Drainage; Experimentation; Pipes; Transient flow; Unsteady flow.

Introduction

The objective of this paper is to present and explain pipeline emptying experiments carried out on the Deltares dynamic multi-phase test rig, configured as a PVC pipeline of nominal 250 mm diameter and 275 m long. Emptying of pipelines, involving interaction between air and water in pressurized systems, occurs in hydraulic applications such as water-distribution networks, stormwater and sewage systems, firefighting systems, and fluid-transport pipelines. With "blow-down" compressed air supplied from upstream, the moving water column is initially pressurized, but it is observed that a stratified water-air "tail" with free-surface flow will form, i.e., mixed pressurized-free-surface flows occur (gravity-driven emptying of the pipeline due to siphon only is not analyzed here). The primary objective is to provide data for future validation of advanced numerical models, but a secondary objective is to use simple models to help interpret the phenomena observed because the scale of this experiment (intended to give higher Reynolds numbers that are more representative of real applications) makes practical flow visualization problematic.

Transient changes in the flow rate and pressure for the simultaneous occurrence of free-surface and pressurized flows in partially filled pipelines can be modeled at varying levels of complexity (e.g., Benjamin 1968; Nydal and Andreussi 1991; Bozkus and Wiggert 1991, 1997; Bozkus et al. 2004; Politano et al. 2005; Vasconcelos et al. 2006; Vasconcelos and Wright 2007; Bourdarias and Gerbi 2007; Leon et al. 2009, 2010; Kayhan and Bozkus 2011). In the case of pipe filling, several types of pressure oscillations may be present, depending on the pipe-end ventilation condition (Zhou et al. 2002). In pipelines with an undulating elevation profile, column separation may occur at high points, and air pockets may be trapped locally (Liou and Hunt 1996). Local and distributed cavitation conditions occur when the liquid pressure drops to the vapor pressure (Bergant and Simpson 1999; Bergant et al. 2005, 2006). With transient flow in plastic pipes (as in these experiments) the viscoelasticity of the pipe wall can be important as compared to the liquid elasticity, resulting in pressure wave attenuation (Bergant et al. 2008a, b).

The pipeline apparatus used in this experimental study is briefly described. Steady-state flows (for measurement of head losses) and transient emptying measurements for a series of runs in different conditions are then presented and interpreted. Measured flow rates, pressures, and water levels are used to determine the transition from full to stratified flow (intrusion of air on top of the water column). Nondimensional key parameters of the emptying system are established. Control volume (CV) model solutions are used to support the interpretation of the observed motion of the air-water front

[1]Associate Professor, Dept. of Mechanics, Tallinn Univ. of Technology, Ehitajate tee 5, 19086 Tallinn, Estonia (corresponding author). E-mail: janek.laanearu@ttu.ee

[2]Teaching Assistant, Dept. of Mechanics, Tallinn Univ. of Technology, Tallinn, Estonia.

[3]Professor, Dept. of Mechanics, Tallinn Univ. of Technology, Tallinn, Estonia.

[4]Litostroj Power d.o.o., Litostrojska 50, 1000 Ljubljana, Slovenia.

[5]Litostroj Power d.o.o., Ljubljana, Slovenia.

[6]Dept. of Mathematics and Computer Science, Eindhoven Univ. of Technology, P.O. Box 513, 5600 MB Eindhoven, The Netherlands.

[7]Assistant Professor, Dept. of Mathematics and Computer Science, Eindhoven Univ. of Technology, Eindhoven, The Netherlands.

[8]Senior Lecturer, School of Mechanical and Systems Engineering, Newcastle Univ., Newcastle upon Tyne NE1 7RU, UK.

[9]Deltares, P.O. Box 177, 2600 MH Delft, The Netherlands.

Note. This manuscript was submitted on July 6, 2011; approved on May 11, 2012; published online on May 15, 2012. Discussion period open until May 1, 2013; separate discussions must be submitted for individual papers. This paper is part of the ***Journal of Hydraulic Engineering***, Vol. 138, No. 12, December 1, 2012. © ASCE, ISSN 0733-9429/2012/12-1090-1100/$25.00.

and associated tail-leakage effects. The water-hammer oscillations due to valve opening are recorded but fluid-structure interaction, due to water slug impact with a downstream 90° vertical steel bend (Fig. 1) after the air-water front had left the outlet, is not reported here.

Experimental Setup

In these two-phase flow experiments the pipeline (Figs. 1 and 2) was initially completely filled with water from a supply tower until steady-state flow was achieved. Then the water-column motion was gradually brought to rest by simultaneously restricting the outflow and reducing the inflow into the pipeline. The resulting static water column was pressurized from an upstream air tank—in different runs the pipeline upstream initial pressure was set at gauge pressures varying between 1 and 2 barg (bar gauge). Controlled emptying started by relatively quick opening of a downstream valve. The formation of the air-water front advancing into the water-filled domain of the pipeline was regulated by the downstream outflow conditions. The pressurized water initially filling the pipeline was replaced by air of gradually decreasing pressure during the emptying process. The observed emptying process was considered ended after the air-water front left the pipeline outlet when air penetrated throughout the pipeline, with further draining continuing thereafter by remaining water slugs flushing out of the system.

The test rig consisted of a constant-head water supply tower 25 m high, a high-pressure air tank, PVC pipes (inner diameter 236 mm and wall thickness 7 mm), 0°, 45°, and 90° PVC and steel joints, steel inlet and outlet parts, and a free-surface basement reservoir collecting the drainage water (Fig. 1). The PVC pipeline was connected to the water tower and the air tank via steel pipe branches with the Y-connection of the inlet steel pipes 4 m above the steel T-connection to the water supply tower and 1 m below the steel connection to the pressurized air pipe from the air tank (Fig. 1). Air supply was regulated by a manually operated butterfly valve (DN300) in the air supply pipe (Valve 1 in Fig. 1). An automatically operated cage valve (DN250) at five diameters' distance from Valve 1 was used to pressurize the pipeline apparatus from the air tank. The supply from the water tower was regulated by an automatically operated butterfly valve (DN150) installed in the water-supply vertical steel pipe (Valve 2 in Fig. 1) mounted between the T- and Y-connections. Unintended internal leakage of Valve 2 in its closed position was eliminated by a backup manual butterfly valve (DN200) nearby. The PVC pipeline outlet was connected to a horizontal steel pipe with a vertical bend to a vertical steel pipe 4.5 m above the ground floor (siphon). The manual butterfly valve (DN200) (Valve 3 in Fig. 1) at the downstream end of the vertical steel pipe was used to regulate the outflow conditions. The orifice of Valve 3 was maximally open at 0° position and fully closed at 90° position. Henceforth a series of relative positions from 0°/90° ≡ 0/9 to 50°/90° ≡ 5/9 of Valve 3 are used to characterize the outflow conditions. Emptying of the initially pressurized pipeline was started by rapidly opening the manually operated "open/close" butterfly valve (DN200) mounted at five diameters' distance downstream of Valve 3 in Fig. 1.

The PVC pipeline consisted of six straight sections (Pipe I: 39.88 m, Pipe II: 11.86 m, Pipe III: 66.59 m, Pipe IV: 66.44 m, Pipe V: 12.08 m, Pipe VI: 48.63 m) connected by four 90° PVC elbows of five diameters' radius and one horizontal 180° PVC turn 6.45 m long (inset **b** in Fig. 2). The 180° PVC turn connects the two parallel-laid Pipes III and IV (Fig. 2). The PVC pipeline was fixed to the concrete floor with steel anchors and supported with wooden blocks to reduce sagging. At the upstream end of the pipeline an 8.75-m-long PVC bridge (inset **a** in Fig. 2) was elevated in a vertical plane 1.3 m above the horizontal pipeline axis. The rest of the PVC pipeline was horizontal. The coordinate system reference point ($x = 0$) for the axis along the pipeline in the flow direction was taken to be at the downstream end of the PVC bridge before the upstream end of measurement Section 1 (Fig. 2). The total length of the continuous horizontal PVC pipeline, including the 90° bends and 180° turn, was 261 m (Laanearu and van't Westende 2010). The PVC part upstream of coordinate $x = 0$, including the out-of-horizontal-plane PVC bridge, had a length of 14 m. Downstream of measurement Section 9 there was an 8.0-m-long PVC part

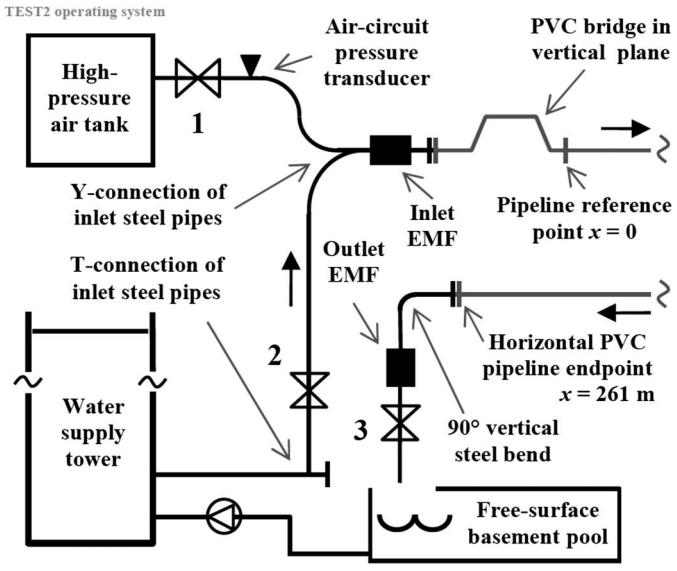

Fig. 1. Test rig operation scheme: 1—manual valve (air supply valve); 2—automatic valve (water supply valve); 3—manual valve (orifice valve) (valves 1, 2, and 3 were used in combination with other valves, not shown here); bold arrows: water flow direction through pipeline

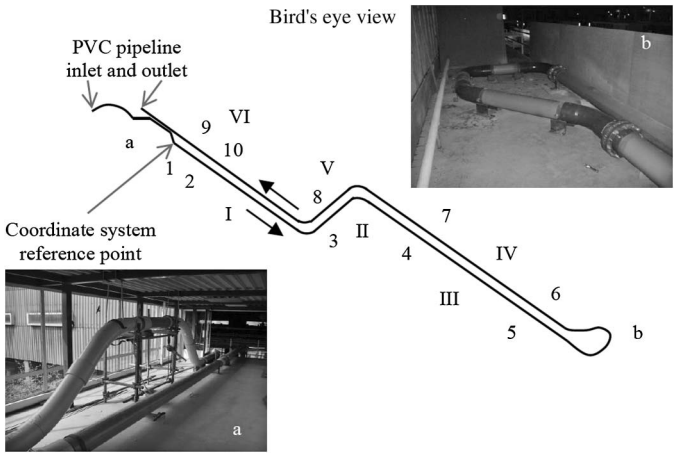

Fig. 2. PVC pipeline layout and instrumentation; locations of measurement sections 1, 3, 5, 6, 7, 8, and 9 and transparent sections 2, 4, and 10; inset **a**: PVC bridge in vertical plane; inset **b**: 180° combined turn in horizontal plane; straight PVC pipes are indicated by roman numerals I, II, III, IV, V, and VI; pressure and water level are measured at sections 1, 3, 5, 7, 8, and 9; temperature is measured at sections 1, 3, and 9; bold arrows: water flow direction through PVC pipeline

J. Hydraul. Eng. 2012.138:1090-1100.

Table 1. Axial Coordinate Position, Measurement Section, Roman Numerals of Straight Pipe Sections and Cross-Sectional Position of Pressure, Water Level, Temperature, and Flow-Rate Measurement Devices

#	Mark	Axial position (m)	Measurement section	Straight pipe	Cross-sectional position
1	P1	1.55	1 (pressure, 0–5 barg)	I	Right side
2	P3	46.59	3 (pressure, 0–5 barg)	II	Bottom
3	P5	111.72	5 (pressure, 0–5 barg)	III	Right side
4	P7	183.72	7 (pressure, 0–5 barg)	IV	Right side
5	P8	206.83	8 (pressure, 0–5 barg)	V	Right side
6	P9	252.76	9 (pressure, 0–5 barg)	VI	Right side
7	WL1	1.67	1 (water level, 12.163 mm/V)	I	Top to bottom
8	WL3	46.39	3 (water level, 12.315 mm/V)	II	Top to bottom
9	WL5	111.72	5 (water level, 12.318 mm/V)	III	Top to bottom
10	WL7	183.72	7 (water level, 11.932 mm/V)	IV	Top to bottom
11	WL8	206.83	8 (water level, 12.246 mm/V)	V	Top to bottom
12	WL9	252.88	9 (water level, 12.178 mm/V)	VI	Top to bottom
13	T1	1.55	1 (temperature, 0–50°C)	I	Left side
14	T3	46.39	3 (temperature, 0–50°C)	II	Right side
15	T9	252.76	9 (temperature, 0–50°C)	VI	Left side
16	Inlet EMF	−14.40	Between steel and PVC pipes (flow rate, 0–500 lps)	Before I	Joint between horizontal pipes
17	Outlet EMF	269.84	Steel pipe (flow rate, 0–500 lps)	After VI	Joint between vertical pipes

Note: See also locations of measurement sections and straight pipes in Fig. 2; flow-meter locations are shown in Fig. 1.

connected to two (horizontal and vertical) steel-pipe parts with a total length of 10.6 m (Fig. 2).

Measurements of pressure (flush-mounted strain-gauge transducers) and pipe internal water level (conductivity probes) along the PVC pipeline were taken at six locations and temperature (platinum resistance sensors) at three locations (Table 1). All measurement sections had a length of 2 m, and the transparent sections had lengths of 0.7 m with transparent windows 0.5 m long. Flow rates were recorded by two electromagnetic flow meters (EMFs) located at the horizontal inflow steel—PVC pipe connection and at the vertical outflow steel-pipe section (Fig. 1 and Table 1). Uncertainty was ±1.0% in flow-rate measurements, ±0.08% in pressure measurements, and ±0.8°C in temperature measurements. Measurement uncertainty in water-level recordings was ±15 mm. The transparent Sections 2 and 10 (Fig. 2) were used to calibrate the water-level measurements with the Sony DXC-990P photo images. A sampling rate of 100 Hz was used to record the experimental quantities: inflow and outflow discharges, gauge pressures, water levels, and temperatures.

Hydraulic Measurements

Steady-State Flow

Prior to the principal pipeline-emptying experiments, steady-state flow measurements were carried out to determine the head losses in the pipeline apparatus. The Darcy-Weisbach equation was used to estimate the friction factors f and minor-loss coefficients K for different sections along the PVC pipeline. The measured flow rates at the upstream and downstream ends, together with time-averaged pressure heads recorded with Transducers P1 and P5 (Table 1), were used to calculate values of friction factor f_{P1-P5}. The minor-loss coefficient $K_{180°}$ of the 180° turn (inset **b** in Fig. 2) was calculated using the measured head loss of the pipeline section between the pressure Transducers P1 and P7, knowing the velocity head from the flow-rate measurements. The results from nine steady-state flow experimental runs confirm that the head loss due to the 180° turn ($K_{180°} = 0.0574$ at Reynolds number 948,000) can be ignored as a first approximation. The measured flow rates, together with time-averaged pressure-heads from Transducers P1 and P9, were then used to calculate the values of the friction factor f_{P1-P9}. The experimentally determined friction factors for all sections including the 90° bends were nearly the same. Given the Reynolds number R and the corresponding friction factor f, the pipe relative roughness (i.e., ratio of equivalent wall roughness size to pipe diameter) k/d can be calculated from the Swamee-Jain approximation to the Colebrook-White formula. For steady-state flows with maximally open end (Valve 3 in Fig. 1) and Reynolds number 948,000, the calculated friction factor is $f_{P1-P9} = 0.0136$ with corresponding relative roughness $k/d = 0.00011$, giving an estimated pipe wall roughness of $k \sim 0.026$ mm. In comparison with the usual PVC pipe roughness size [e.g., ~0.0034 mm in Liou and Hunt (1996)], the pipe friction factor at Reynolds number $\mathsf{R} = 950{,}000$ would be $f = 0.0117$. Accordingly, the PVC pipeline used in the experiments is characterized by a comparatively large equivalent roughness as it was built from 10-m-long PVC pipes that are connected with 45 and 90° PVC bends of different radii due to the rather complicated layout configuration (Fig. 2) over the ~0.3 km distance between different buildings (*Stromingslaboratorium* and *ZoutZoet Hal*) in Delft. The water temperature varied between 17.3 and 18.4°C in the experiments.

Water Hammer

The pipeline emptying measurements, though focusing on relatively slow flow changes, included also initial fast transient effects. To complete the preliminary pipeline characterization, elastic characteristics were investigated separately from the principal pipeline-emptying experiments. For this purpose a bypass valve was installed at the downstream end of the pipeline apparatus, in the vertical steel pipe, and 1 m above the ground floor. Before each water-hammer test the same initialization procedure to fill the pipeline as for the emptying experiments was used, but the air supply was well closed and care was taken to ensure air was removed from the pipeline. Water-hammer pressure waves were generated with bypass valve opening and closing procedures guaranteeing a safe pressure range. The experimentally determined pressure-wave celerity in the PVC pipe between measurement Sections 1 and 9 was about 350 m/s (Bergant et al. 2011). This measured estimate of comparatively low pressure wave speed is characteristic of PVC pipes.

J. Hydraul. Eng. 2012.138:1090-1100.

Table 2. Experimental Quantities for Representative Runs 1–9

Run	Initial air-circuit pressure (barg)	Valve 3 opening	H_{air} (m) (dH_{air}/dt, m/s)	$\tau_{(1)-(9)}$ (s)	K_{end}	h_p/h_f	**Zu**
1	2.0	0/9	19.60 (−0.114)	37.2	3.32	1.074	0.45
2	1.5	0/9	14.90 (−0.815)	44.8	3.50	1.072	0.58
3	1.0	0/9	9.80 (−0.051)	50.9	3.48	1.080	0.58
4	2.0	1/9	20.10 (−0.119)	36.0	3.64	1.042	0.33
5	2.0	3/9	20.00 (−0.105)	39.8	5.88	1.061	0.43
6	2.0	5/9	19.65 (−0.063)	53.8	21.24	1.057	0.42
7	1.0	1/9	10.05 (−0.058)	46.0	3.84	1.067	0.44
8	1.0	3/9	10.00 (−0.051)	49.6	6.14	1.077	0.39
9	1.0	5/9	9.80 (−0.033)	68.6	22.68	1.066	0.49

Note: Initial air-circuit gauge pressure and downstream-end valve opening positions are given. Initial driving pressure-head is H_{air} and dH_{air}/dt corresponds to its dropping rate. $\tau_{(1)-(9)}$ is the measured period of the air-water front traveling between measurement Sections 1 and 9. The pipeline downstream end minor loss coefficient K_{end} is given at Reynolds number 950,000. The parameter h_p/h_f represents the ratio of driving pressure-head difference and frictional head loss, and **Zu** is the corresponding Zukoski number (h_p/h_f and **Zu** are given at the instant of the minimum flow acceleration $(du/dt)_{min}$).

Emptying

The initial condition for each emptying experiment was well established because the pipeline was fully filled and the static-water column was pressurized from the high-pressure air tank. Each emptying experiment was started by a relatively rapid (manual) opening of the valve mounted downstream of Valve 3 (Fig. 1). Water was driven out of the pipeline by compressed air from the upstream high-pressure tank (pressure initially fixed to 1, 1.5, or 2 barg). The pipeline outflow conditions were fixed at four positions (0/9, 1/9, 3/9, and 5/9) of the butterfly Valve 3 (Fig. 1). The principal focus was on the air-water front (also the trailing edge of the moving water column) traveling between measurement Sections 1 and 9 (Fig. 2). The air-water front in this study is defined as the last planar (full of water) cross section separating the empty/stratified and fully filled parts of the PVC pipeline.

The driving air pressure diminished gradually (more or less linearly) during the emptying process (Table 2). The outflow rates Q_{outlet} (outlet EMF in Fig. 1) versus the driving air-pressure head H_{air} (air-circuit pressure transducer in Fig. 1) of the representative Runs 1–9 are presented in Fig. 3, with the transient-flow rates shown in Fig. 4. The initial flow oscillations were due to water hammer caused by rapid valve opening. Fig. 5 shows the measured water level (WL3 in Table 1) history of the water-air tail. The pipeline was fully filled (to its internal diameter of 236 mm) before the air-water front intruded from the PVC bridge into the horizontal part of the PVC pipeline. The presence of stratified flow is clearly evident from Fig. 5 because the water level remains above the pipe-bottom level after the arrival of air at each measurement section, with all experiments confirming that the flow at measurement Sections 3, 5, 7, 8, and 9 remained stratified after the air-water front had passed. The terminology "stratified" is used herein in the context that a clear distinction is observed visually between the water in the lower part of the pipe and the air in the upper part of the pipe with nearly horizontal definite interface in the transparent Sections 4 and 10 (Fig. 2). The air-water front motion between measurement Sections 1 and 9 lasted from 35 to 70 s in the different Runs 1–9 (Table 2). The camera images indicated the change of phase, but, due to water-film formation on the transparent walls, the air-water front itself was poorly visualized. Almost planar motion of the air-water "interface" was only observed at measurement Section 1, and the stratification due to the intrusion of the air along the top surface of the water column occurred before the air-water front passed measurement Section 3 in all runs observed. Fig. 5 confirms that for all runs the stratified flow itself was complex, with temporally diminishing depth of flow and with the appearance of surface waves.

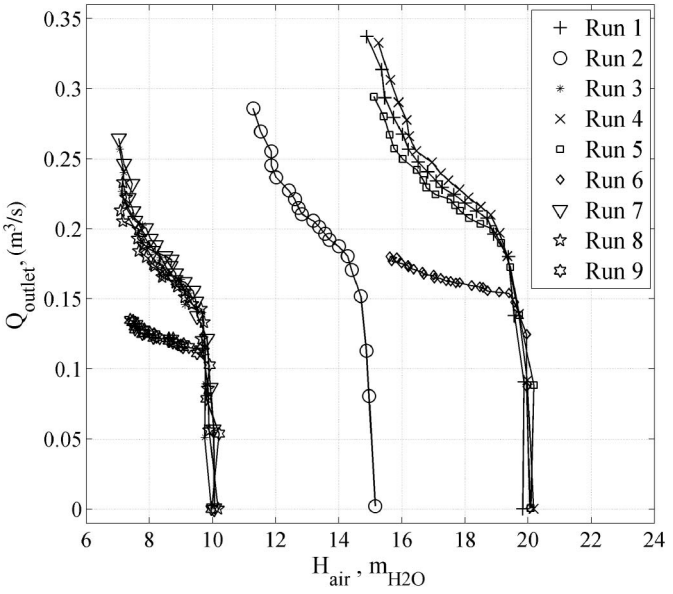

Fig. 3. Measured outlet water discharge Q_{outlet} (outlet EMF in Fig. 1) versus driving air-pressure head H_{air} (air-circuit pressure transducer in Fig. 1) during emptying of PVC pipeline (plotted with frequency 0.4 Hz) [initial air-circuit gauge pressure and downstream valve 3 (Fig. 1) opening position are in Table 2]

The measurements of flow rate, pressure, and water level were subjected to fluctuations (mechanical noise) associated, apparently, with vibrations of the pipeline apparatus. To check the repeatability of the measurements, a series of five runs was carried out with the same driving air pressure and outflow conditions. An example of five pressure recording repetitions at measurement Sections 1 and 9 (for representative Run 4) and overall means are shown in Fig. 6. Apart from the initial pressure oscillations due to water hammer resulting from downstream valve opening, the repeatability of the experiments with the same driving pressure and outflow conditions is considered acceptable. The coefficient of variance, determined for all runs, at measurement Sections 1–9, is around 7%.

Examination of these pipe-emptying measurements reveals that

1. Rapid (within 0.1 s) manual opening of the downstream valve (at five diameters' distance downstream of Valve 3 in Fig. 1)

J. Hydraul. Eng. 2012.138:1090-1100.

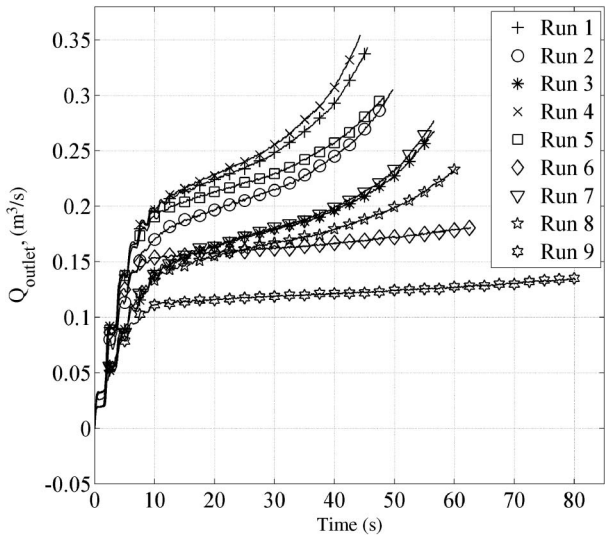

Fig. 4. Flow rate Q (outlet EMF in Fig. 1) measurements from rest until the instant when air arrived at measurement section 9 for representative Runs 1–9 (plotted with frequency 0.4 Hz)

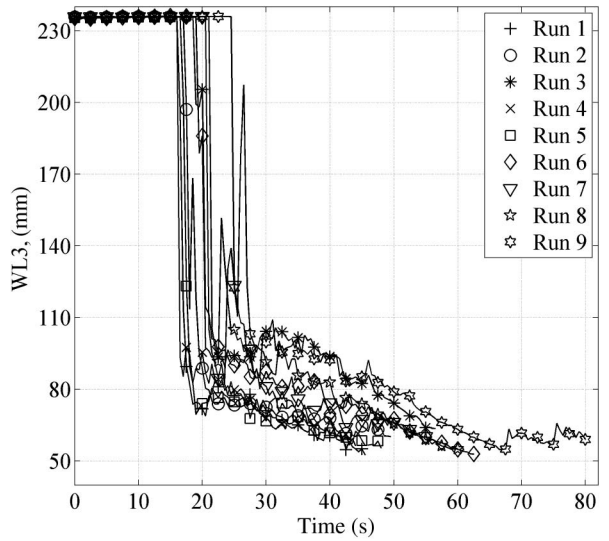

Fig. 5. Water level at measurement section 3 (WL3 in Table 1) during pipeline emptying for representative Runs 1–9 (plotted with frequency 0.4 Hz) (reference time $t_0 = 0$ is at opening instant of downstream valve)

affects the emptying process dynamics in terms of a water hammer for a period of about 15 s, during which large-amplitude pressure oscillations occur and the outflow increases stepwise.

2. Flow-rate measurements (outlet EMF in Fig. 1) represent the rigid water-column velocity well after the water hammer (i.e., water-column vibration) is damped out (Fig. 4).
3. Pressure transducers along the pipeline clearly detect the water-column motion until air arrives at the measurement sections.
4. The decrease of the driving air pressure is almost linear in time and practically uniform instantaneously along the pipeline.
5. Water-level measurements indicate flow stratification (free surface) after the passing of the air-water front as a result of air intrusion, and the term *tail leakage* is used henceforth to refer to the gradual depletion of the water column.

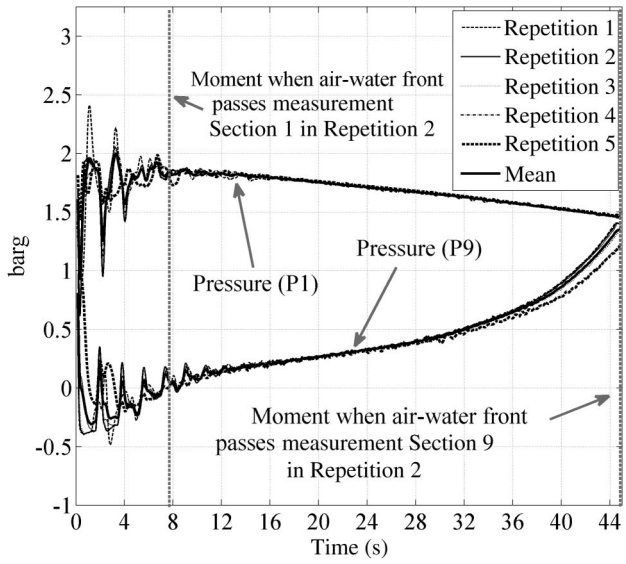

Fig. 6. Measurement sections 1 and 9 pressure recordings (P1) and (P9), and overall means. Representative Run 4 corresponds to repetition 2; in all repetitions (1–5) the air-water front is traveling to measurement section 9 (Fig. 2), starting at rest ($t_0 = 0$)

Discussion of Measurements

Measurements indicate that the phenomena that characterize this dynamic system are as follows:

1. Air-water interaction, i.e., water is replaced by air with the trailing edge of the moving water column leaving stratified flow behind it (Fig. 5). The standard 1D model assumption is that there is a well-defined planar air-water front, which can be the case in a vertical pipe in which surface-tension effects are negligible. However, this assumption is not valid for a horizontal pipe of sufficiently large diameter, where the air is largely confined to the upper part of the cross section and water occupies only the lower part, as is the situation for long bubbles moving due to gravity in a closed horizontal tube (e.g., Zukoski 1966; Benjamin 1968). The planar air-water front approximation is reasonable in a 1D model (Leon et al. 2010) if the horizontal extent of the front is short, as was observed in the emptying experiments at transparent Section 2 (Fig. 2).
2. The pipeline emptying flow is unsteady (Fig. 4) and involves changes in driving pressure (Fig. 6), water inertia, and skin friction. The flow acceleration is directly related to the pressure gradient at startup because at this early stage of the unsteady flow the magnitudes of the pressure-gradient force and the inertia force are both much larger than the friction force (Koppel and Ainola 2006; Annus and Koppel 2011). The effects due to molecular viscosity and surface tension are not important in pipes of large diameter (Liou and Hunt 1996).

Dimensional analysis suggests that there are four key parameters characterizing turbulent stratified compressible flows:

$$\mathrm{R} = \frac{4Q\rho}{\pi d\mu} \quad \text{Reynolds number} \tag{1}$$

$$\mathrm{F} = \frac{u}{\sqrt{gd}} \quad \text{Froude number} \tag{2}$$

$$\mathbf{Zu} = \frac{c}{\sqrt{gd}} \quad \text{Zukoski number} \tag{3}$$

J. Hydraul. Eng. 2012.138:1090-1100.

$$\mathsf{M} = \frac{u}{a} \qquad \text{Mach number} \tag{4}$$

Water density is ρ, dynamic viscosity is μ, acceleration due to gravity is g, either pipe inner diameter or the centerline water depth is d, pressure-wave celerity is a, flow rate is Q, flow velocity is $u = 4Q/(\pi d^2)$, and air-cavity celerity is c. The estimated Reynolds number values for the fully filled section during emptying of the horizontal PVC pipeline between measurement Sections 1 and 9 (Fig. 2) varied in the range $\mathsf{R} = (0.54\text{–}1.91) \times 10^6$. The estimated values of Froude number and Mach number varied in the range $\mathsf{F} = 1.51\text{–}5.35$ and $\mathsf{M} = (0.66\text{–}2.32) \times 10^{-2}$, respectively. Therefore, the effects of a water hammer can be ignored as a first approximation for slowly accelerated flow (cf. Bozkus et al. 2004). The Froude number of the stratified water-air "tail" behind the water column was assumed small [$\mathsf{F} \sim 0$ when the parameter d in Eq. (2) for free-surface motion behind the air-water front is the centerline water depth]. The Reynolds, Froude, and Mach numbers are proportional to the flow velocity and, hence, outflow rate. The Zukoski number introduced here characterizes air intrusion on top of the moving water column, which—alternatively—can be interpreted as water-tail leakage. It is apparent that air intrusion occurs when a long air cavity develops in a pipeline, with a closed end upstream and an open end downstream, drained under gravity (Benjamin 1968; Zukoski 1966). The experimentally estimated Zukoski number maximum values varied here in a range of $\mathbf{Zu} = 0.48\text{–}1.05$. In Zukoski's (1966) experiments $\mathbf{Zu} \approx 0.53$ for a horizontal tube with diameter 178 mm and length-to-diameter ratio 20:1.

The measured outflow rates showed a continuously increasing velocity of the shortening water column. The flow in the pipeline was mainly driven in two stages: first the flow was accelerated from rest and after some period, then the flow experienced an acceleration minimum, which was followed by speeding up until the pressurized air flushed out the remaining pressurized water column from the outlet. The minimum of water-column acceleration $(du/dt)_{\min}$ was identified by the inflection point ($d^2u/dt^2 = 0$) in the outflow rate curve (Fig. 4). Some experimental results are presented in Table 2, with values of the parameters h_p/h_f and $\mathbf{Zu}$ corresponding to the instant of unsteady flow with the minimum flow acceleration $(du/dt)_{\min} = (0.5\text{–}4.5) \times 10^{-2}$ m/s^2, where h_p = time-dependent pressure head of the air phase relative to the pressure head at the outlet and $h_f = fLu^2/(2gd)$ = frictional head loss calculated from the Darcy-Weisbach equation for fully water-filled pipe section of length L and friction factor f. The results presented in Table 2 confirm that the minimums of parameter h_p/h_f do not match with the quasisteady flow conditions, i.e., the flow with changing acceleration did not become steady during the emptying process. In the experiments, three processes were occurring concurrently. The driving air pressure was decreasing. At the same time the combination of the pipe-end drainage and tail leakage behind the moving air-water front were decreasing the size of the pressurized water column and, hence, both its inertia and the frictional head losses, this latter being an inverse result from the pipeline-filling study of Liou and Hunt (1996). The frictional head loss initially increased, but after the point of inflection in the flow-rate curve (Fig. 4) it decreased in the pipeline-emptying experiments analyzed.

The equilibrium of forces in the fully water-filled straight pipe for unsteady flow with constant acceleration starting from rest and associated flow transition to turbulence was studied in Annus and Koppel (2011). In the cases of maximally open downstream valve Positions 0/9 and 1/9 (Runs 1–4 and 7), the water column's initial and final accelerations were both large compared to the acceleration minimum. The initial acceleration of the moving water column was larger (over 5 times) than the final flow acceleration for partial opening of the downstream valve (3/9 and 5/9, Runs 5–6 and 8–9). The final accelerations in Runs 6 and 9, corresponding to the most restricted outflow due to partial opening (5/9) of the downstream valve, were close to the minimum accelerations $(du/dt)_{\min} = 9.4 \times 10^{-3}$ m/s^2 and 4.9×10^{-3} m/s^2, respectively. It can be concluded that the inertia force due to flow acceleration was important at the start of the flow in all emptying runs under investigation, and the inertia effects due to tail leakage and pipe-end drainage became important in the final stage of pipeline emptying.

In the different runs analyzed, the minimums of flow acceleration (corresponding to "inflection points of the flow-rate curve" in Fig. 4) occurred after the air-water front passed measurement Section 3 (Fig. 2), positioned approximately 47 m from the coordinate datum ($x = 0$) at the PVC bridge outlet. Stratified flow was not observed during the emptying process at measurement Section 1 but first appeared at measurement Section 3 (Fig. 5). The initiation of tail leakage of the water column, which corresponds to flow stratification due to air intrusion on top of the water column, thus occurred between measurements Sections 1 and 3 (Fig. 2). This may be important in several aspects, but it could not be visually observed due to the limited number of transparent sections (Fig. 2). The slope dd/dx of the water-air tail surface (Fig. 5) tends to decrease over time (as in a wave rarefaction with the smaller d-values part of the free-surface flow upstream, propagating more slowly than those with the larger d-values part downstream). The breaking head waves (Benjamin 1968) occur when the free-surface flow is supercritical, i.e., the local Froude number is larger than unity ($\mathsf{F} > 1$). In the emptying experiments, the air flow on top of the free-surface water continuously accelerated until the stratified flow in the pipeline experienced destabilizing conditions (formation of incidental water slugs), after the pressurized water column was flushed out of the outlet.

Control Volume Model Interpretation

Due to the practical constraint of not being able to visually observe the physical development of the tail leakage in these experiments, some simple modeling was undertaken in an attempt to clarify what phenomena might be involved, though the intention is not to accurately represent the free-surface flow region. The accelerating and shortening control volume, containing water that fully fills the pipeline cross-sectional area up to the outlet (Fig. 7), has fixed surfaces at the pipeline walls and at its outlet at a position 18.6 m downstream of measurement Section 9 (Fig. 2). A control surface 11 at the "last" fully filled cross section moves as the air-water front between measurement Sections 1 and 9 in Fig. 2, where a surface 99 is fixed at measurement Section 9. Without tail leakage, control surface 11 moves at a velocity given by the rigid water-column velocity $U = Q_{\text{outlet}}/A$. The length of the water-column part between control surface 11 and surface 99 is $l(t)$, and the length of control volume is $L(t) = l(t) + 18.6$ m. Due to tail leakage, control surface 11 advances more rapidly than the water-column velocity $U(t)$. Applying conservation of momentum and volume to the CV in Fig. 7, the following equation results:

$$\frac{dU}{dt} - g\frac{(h_p - h_f)}{L} = \beta\left(\frac{1}{\alpha} - 1\right)\frac{U^2}{L} - \frac{U^2}{L} \tag{5}$$

where h_f = instantaneous Darcy-Weisbach quasisteady friction head loss and h_p = pressure-head difference between the moving control surface 11 and the pressure head at the pipeline outlet

J. Hydraul. Eng. 2012.138:1090-1100.

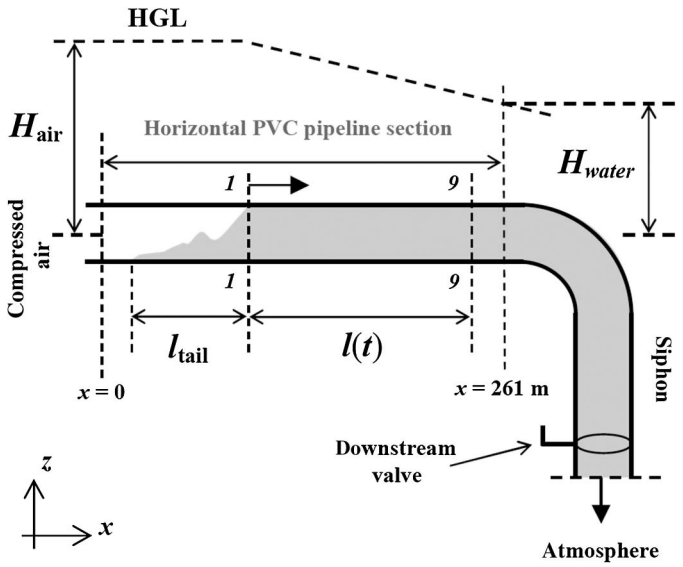

Fig. 7. Schematic and coordinate system of pipeline; water-air tail length l_{tail} and horizontal water-column part length l (between surfaces 11 and 99) are indicated during emptying process [CV length corresponds to fully water-filled pipeline section of length $L(t) = l(t) + 18.6$ m]; pressure head in compressed air section and at PVC pipeline outlet is H_{air} and H_{water}, respectively (Fig. 2)

(due to a siphon effect and outflow conditions), and the model coefficients vary in the ranges $0 < \alpha < 1$ and $\beta > 2$. The mass loss is included as a hold-up coefficient α, so that the amount of mass lost per unit length is $\rho(1-\alpha)A$. The residual momentum changes due to boundary and internal motion relative to the CV in Eq. (5) are accounted for by the coefficient $\beta = 1 + \alpha/(1-\alpha)(1/U^2)\int_{residual}(\partial U_r/\partial t)ds$, where U_r = relative velocity. In the case of liquid slug motion in a voided line, this coefficient is related to the hold-up coefficient α by a functional relationship $\beta = 2 + \alpha/(1-\alpha)$ (cf. Bozkus and Wiggert 1997).

The right-hand-side terms in Eq. (5) allow investigation of an unsteady flow with tail leakage, with the limitation that water is at rest behind the air-water front (i.e., $F = 0$); in addition, backward-directed flow in these emptying experiments would have been almost absent due to the air shear-stress effects on the surface of the stratified flow. The shortening of the control-volume length L due to tail leakage and drainage is given by conservation of volume:

$$\frac{dL}{dt} = -\left(\frac{1}{\alpha} - 1\right)U - U \tag{6}$$

It was experimentally observed that stratified flow was absent at measurement Section 1 but appeared at measurement Section 3 (Fig. 5) and other sections during the emptying process. Thus the water-column tail leakage started at an instant $t_{tail\text{-}leakage} = t_0 + \Delta t$, measured from the reference time t_0 and with Δt representing the short period of motion with a planar air-water front. Modeling pipeline emptying during the period Δt without tail leakage leads to the simplified case where $\alpha = 1$ in Eqs. (5) and (6) and β is assumed constant. This model is similar to that of Zhou et al. (2002) and describes rigid nonleaking water-column motion. The reference time $t_0 = 0$ for all Runs 1–9 is taken to be the opening instant of the downstream valve. Experimentally known boundary and initial conditions (Table 2) are adopted in the CV model calculations, namely, the gradually reducing driving air pressure and the flow-rate-dependent pressure at the outlet.

In principle, the discrepancies between the stratified and nonstratified pressurized flows should be resolved using the full set of Eqs. (5) and (6), i.e., including the tail-leakage terms in the numerical calculation. The standard fourth-order Runge-Kutta numerical scheme was employed for the simultaneous solution of Eqs. (5) and (6), representing the water-column motion first without tail leakage (nonstratified flow case with planar air-water front) and then with tail leakage (stratified flow case). An iterative procedure was included in the numerical calculation to determine the coefficient α for a constant β by fitting the flow rate (approximated from measurements and ignoring the water hammer) at different times during emptying. In the model calculation, control surface 11 reaches the surface 99 position (Fig. 7) at the same time as the air-water front in the corresponding experiment reaches measurement Section 9. The estimated coefficient β values are presented in Table 3, and the hold-up coefficient α varied in the model calculations between $0.5 < \alpha < 1.0$ (consistent with the water-level measurements in Fig. 5). An example of the calculated flow rates, corresponding to Run 2, for these stratified $0.5 < \alpha < 1.0$) and nonstratified ($\alpha = 1$) cases is presented in Fig. 8. As in the measured situation, the water initially present in the pipeline is replaced by pressurized air during the motion of control surface 11 toward the surface 99 position. The simulated flow is also driven in two stages during the emptying period (Fig. 8). First, the flow is accelerated from rest, and after some period the acceleration experiences a minimum, followed by increasingly accelerated flow until the air phase reaches surface 99, mimicking the observed behavior. However, the pipeline-emptying period calculated only for $\alpha = 1$ overestimated

Table 3. Experimental and Model Results of Representative Runs 1–9

Run number	$u_{(1)}$(m/s)	$u_{(9)}$(m/s)	x_i(m)	α	β	$l_{tail,measured}$(m)	$l_{tail,modeled}/l_{tail,measured}$ (%)
1	4.18	7.90	−16.2	0.88	6.4	44.0	76.9
2	2.83	7.04	−20.8	0.84	4.6	47.2	95.5
3	2.29	6.20	−20.7	0.82	3.9	53.8	93.2
4	4.20	8.13	−14.7	0.91	11.3	44.0	56.3
5	4.07	6.91	−14.7	0.88	6.3	46.1	69.2
6	3.43	4.16	−13.1	0.85	4.5	60.6	62.7
7	3.20	6.38	−12.9	0.85	5.8	48.3	81.6
8	3.09	5.42	−13.8	0.86	5.0	55.0	77.2
9	2.55	3.09	−15.8	0.79	2.7	68.8	76.3

Note: $u_{(1)}$ and $u_{(9)}$ are the measured outflow velocities at the instant when the air-water front passes measurement Sections 1 and 9, respectively; x_i (Fig. 2) is the initial air-water front coordinate; α and β are the CV model coefficients [α is given only at the instant of the minimum flow acceleration $(du/dt)_{min}$; cf. Fig. 8]; $l_{tail,measured}$ and $l_{tail,modeled}$ are the measured and predicted tail-leakage lengths (as percentage of measured length), respectively, given by the tail-water volume per pipe cross-sectional area, at the instant when the air-water front passes measurement Section 9.

J. Hydraul. Eng. 2012.138:1090-1100.

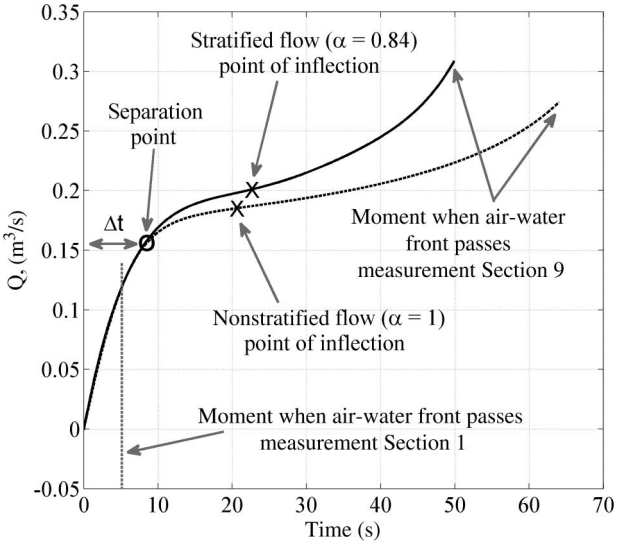

Fig. 8. Calculated flow rates for stratified ($0.5 < \alpha < 1.0$) and nonstratified ($\alpha = 1$) cases, corresponding to representative Run 2; the instant when the air-water front passes measurement section 1 is indicated by a dashed vertical line; Δt represents the short period of water-column motion with a planar air-water front in the CV model; the instant when the stratified (solid curve) and nonstratified (dashed curve) flow-rate curves start to diverge is represented by the point of separation, indicated by a circle (o); the stratified (that is, with tail leakage) and nonstratified case points of inflection are shown by crosses (x)

the measured emptying period in all Runs 1–9 because the solution (dashed curve in Fig. 8) corresponded to the planar air-water front motion without tail leakage. The correlation between the stratified (solid) and nonstratified (dashed) flow-rate curves in Fig. 8 is initially comparatively good but diverges significantly as the emptying process progresses. The instant when the flow rates for these two cases diverge is indicated by a "separation point" in Fig. 8. In the different runs analyzed, the separation point, representing essentially the start of water-column tail leakage, occurred between measurement Sections 1 and 3, confirming the experimental observations.

It was found that the cumulative water-column leakage in the calculation, given by the "modeled" tail-leakage length $l_{\text{tail,modeled}}$, underestimated the "measured" tail-leakage length $l_{\text{tail,measured}}$ (estimated from the measured cumulative free-surface flow volume behind the air-water front) to a varying extent (Table 3). This comparison showed if tail leakage was included in the CV model, then the stratified-flow simulations corresponded in their general features to the measured flow rates in all Runs 1–9 analyzed, and the water levels and pressures (ignoring the water hammer) in the CV model also corresponded quantitatively well with the experimental results after the "inflection point" instance of the flow-rate curve. This suggests that the mismatch of the *modeled* and *measured* stratified ($0.5 < \alpha < 1.0$) mass-loss volumes was apparently due to the complex (but only partially observable) nature of the free-surface dynamics behind the air-water front (cf. Nydal and Andreussi 1991).

The aim of this CV model approximation was the interpretation of the relatively slowly accelerating water column. It can be

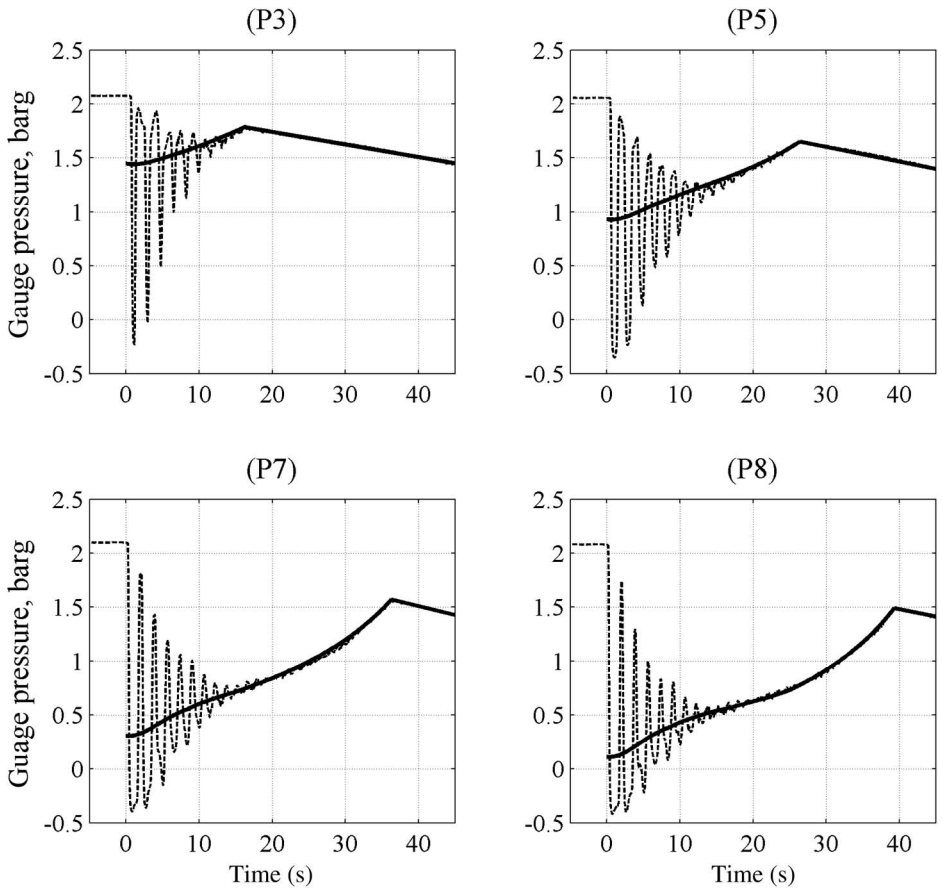

Fig. 9. Dashed curves: measured Pressures P3, P5, P7, and P8 of representative Run 4; the pressure fluctuations in measurement sections 3, 5, 7, and 8 are due to downstream valve opening; bold solid curves: CV model pressures for slowly accelerated flow

J. Hydraul. Eng. 2012.138:1090-1100.

concluded that in all Runs 1–9 analyzed the pressurized air intrusion into the pipeline was strongly affected by the flow stratification. Formation of almost horizontal water surface was apparent from the water-level height at measurement Sections 3, 5, 7, 8, and 9 (Fig. 2). At measurement Section 1 the water-level height (WL1 in Table 1) was close to zero during the emptying process, indicating that initially a planar air-water front entered the horizontal pipeline from the PVC bridge outlet. Therefore, the measured instant of minimum flow acceleration always occurred after the start of water-column tail leakage. The air-cavity celerity $c = U(1-\alpha)/\alpha$, defined by the relative shortening velocity of the water column due to tail leakage, was zero ($\alpha = 1.0$) till the instant of the separation point (Fig. 8), after which the flow was stratified ($0.5 < \alpha < 1.0$) and the celerity c was not zero.

Evaluation of Fast Transient Issues

Examples of water-hammer pressure oscillations at measurement Sections 3, 5, 7, and 8 for Run 4 are shown in Fig. 9 (see also Fig. 6), which suggests that the final emptying process in the different runs was not significantly affected by the water-hammer high-frequency pressure fluctuations, though the outflow-rate measurements in Fig. 4 also exhibit water-hammer fluctuations. The damping of the water-hammer oscillation was mainly due to the viscoelasticity of the PVC pipe wall (Bergant et al. 2011) and the increasing acoustic wave frequency due to the shortening of the pressurized water column between the moving air-water front and the pipeline downstream end (cf. Bergant and Simpson 1999). The effect of unsteady friction on water-hammer waveforms can be significant (Bergant et al. 2008b), but in the case of relatively slowly accelerating flow, such as analyzed in the previous section, quasisteady friction gives most of the frictional dissipation. A slowly accelerating water-column motion in the CV model was determined by the velocity $U(t)$ (corresponding to the pipeline outlet velocity ignoring a water hammer), and due to tail leakage, the air-water front velocity was $U(t)/\alpha$. The CV model pressures (solid curves) for representative Run 4 are also shown in Fig. 9

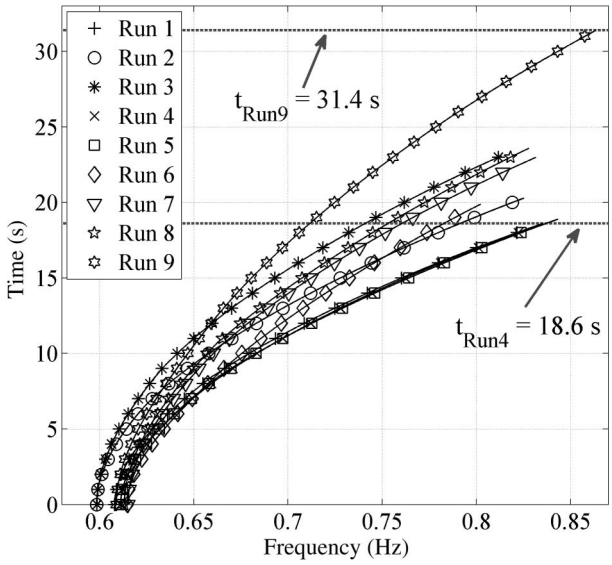

Fig. 10. Simulated water-hammer (acoustic-wave) frequencies of representative Runs 1–9; the water-hammer wave is calculated until the instant represented by the point of inflection in the flow-rate curve (Figs. 4 and 8, solid curve), varying in different Runs between $t_{Run4} = 18.6$ s (Run 4) and $t_{Run9} = 31.4$ s (Run 9)

in comparison with the measured situation, indicating that in the very initial period only the water hammer exists. In the method of characteristics (MOC) calculations of the water-hammer signals (Wylie and Streeter 1993), the air cavity that intrudes on top of the water column can act as a moving boundary, and water-hammer waves with one-direction travel time $L(t)/a$ propagate between the moving air-water front and the pipeline downstream end. The estimated pressure-wave celerity was $a = 350$ m/s (Bergant et al. 2011). The wave paths (cf. Bozkus and Wiggert 1997) corresponding to the water-hammer front (x, t) "zigzag" positions for Runs 1–9 are used to calculate the water-hammer frequency ν_{wh} in Fig. 10, until the instant of the flow-rate curve point of inflection is reached, i.e., in Run 4 until $t_{Run4} = 18.6$ s and in Run 9 until $t_{Run9} = 31.4$ s. The numerical grid and corresponding characteristic lines of the slowly accelerated flow downward (+) and upward (−) direction propagating pressure signals are adapted to the changing water-column length. The right-hand-side boundary in the MOC calculation is fixed to the pipeline outlet, and the left-hand-side boundary (the CV model control surface 11 in Fig. 7) moves together with the air-water front position. The experiments suggest that the water-hammer pressure fluctuations vanished before the instant of the inflection point of the flow-rate curve was reached in all runs analyzed.

Conclusions

The experimental results presented in this study represent a large-scale pipeline "blow-down" emptying process for varying driving pressures and outflow resistances. One aim of the experiments was to investigate relatively slowly accelerated flow in a pressurized pipeline (long enough to neglect the pipeline interior minor losses) with a focus on the air-water front traveling unidirectionally inside the horizontal pipeline. The measured flow was predominantly driven in two stages: first the flow was accelerated from rest, then after some period the flow experienced an acceleration minimum and then speeded up until the pressurized air flushed the remaining pressurized water column out of the pipeline. Experiments showed that in the case of a well-opened pipeline downstream end, the initial and final accelerations of the moving pressurized water column were both large as compared to the acceleration minimum experienced by the unsteady flow. In the case of partial opening, the initial accelerations of the moving pressurized water column were large compared to the final flow acceleration, and in the case of the most restricted outflow, the final stage flow acceleration did not change much compared to the minimum measured flow acceleration. Experimental results indicate that at the instant of minimum flow acceleration of the water-column motion, values of the Zukoski number were close to the critical value whose long air-cavity celerity c is $0.5\sqrt{gd}$ (when the parameter d is pipe inner diameter) according to Liou and Hunt (1996). The acceleration minimum of the water-column motion represents the stage of the unsteady flow where the magnitude of the pressure gradient force and the frictional force are much larger than the force due to inertia.

A simple CV approach was employed to support interpretation of the slowly accelerated emptying flow observations. The water flow was dependent on air pressure, siphoned outflow, frictional resistance, and tail leakage in the CV model. The discrepancy between calculated emptying periods for the stratified and nonstratified water-column motion situations supported experimental evidence of the formation of a water-air tail behind the air-water front advancing inside the pipeline. The general effect of stratification was to speed up the process of air penetrating the outlet. The analysis confirmed the observation that the leaking of the water

J. Hydraul. Eng. 2012.138:1090-1100.

column trailing edge first occurred shortly after compressed air entered the horizontal part of the PVC pipeline. The instant of the minimum flow acceleration (represented by the point of inflection of the flow-rate curve) always occurred after the start of tail leakage in the pipeline. The minimum flow acceleration was essentially dependent on the outflow conditions and was most delayed during the emptying period in the case with the most restricted outflow. However, though this simple model gave qualitative guidance, even considering the water-column mass loss (coefficient α) and associated residual motion (coefficient β) in the CV model equations, the cumulative stratified flow volume estimated in the horizontal part of the pipeline was only partially predicted (56–95% in Table 3), indicating the limitations. This outcome may be due to several factors related to measurement discretization (6 points) and the simple CV modeling approach used (behind the air-water front $\mathsf{F} = 0$ was assumed).

Rather rapid (~0.1 s) opening of the downstream valve briefly affected the emptying process dynamics due to a water hammer. Pressure fluctuations due to a water hammer existed during the pipeline emptying but only for a short period (considerably shorter than the emptying period), being damped completely before the instant the flow-rate curve point of inflection was reached. The water-hammer wave frequency during damping increased, from 0.60 to 0.615 Hz up to 0.81 to 0.86 Hz due to water-column shortening associated with water outflow and air intrusion on top of the water column.

Pipeline-emptying and filling processes involve different types of flow dynamics. The pipeline-filling process in this apparatus (Laanearu et al. 2009) is characterized by comparatively rapid initial acceleration followed by deceleration of flow until the water-column strikes the downstream-end orifice, tending toward steady-state flow after the attenuation of fast transients. However, the emptying runs reported here reveal continuously accelerated shortening water-column situations. The dynamic difference in water-column motions during pipeline emptying and filling is due to the different boundary conditions and resulting balances between the pressure-gradient, frictional, and inertial forces affecting the flow dynamics at different stages. It is concluded that intrusion of air on top of the water column has a significant effect on the dynamics of a moving air-water front in a large-scale pipeline.

Acknowledgments

The project *Transient Vaporous and Gaseous Cavitation in Pipelines* carried out at Deltares, Delft, the Netherlands, was funded through EC-HYDRALAB III Contract 022441 (R113) by the European Union. The authors would like to thank Richard Tuin, Martin Boele, and Theo Ammerlaan for their technical support during the experiments.

Notation

The following symbols are used in this paper:

A = cross-sectional area of flow [m^2];
a = pressure-wave celerity [m/s];
barg = gauge pressure [bar];
c = long air-cavity celerity [m/s];
d = pipe inner diameter (centerline water depth) [m];
F = Froude number [1];
f = friction factor [1];
g = acceleration due to gravity [m/s^2];
H = pressure head [m_{H20}];
h_f = hydraulic head loss [m];
h_p = pressure-head drop [m];
K = minor-loss coefficient [1];
k = equivalent pipe roughness size [m];
L = fully water-filled pipeline section (CV length) [m];
l = horizontal water-column part [m];
l_{tail} = tail-leakage length [m];
M = Mach number;
Q = flow rate [m^3/s];
R = Reynolds number [1];
t = time [s];
U = CV model velocity [m/s];
U_r = CV model relative velocity [m/s];
u = flow velocity [m/s];
x = axial coordinate [m];
$\mathbf{Zu}$ = Zukoski number [1];
α = CV hold-up coefficient [1];
β = CV residual motion coefficient [1];
μ = dynamic viscosity [kg/(m · s)];
ν_{wh} = water-hammer frequency [Hz];
ρ = fluid density [kg/m^3]; and
τ = emptying period [s].

References

Annus, I., and Koppel, T. (2011). "Transition to turbulence in accelerating pipe flow." *J. Fluids Eng.*, 137(7), 071202-1–071202-9.

Benjamin, T. B. (1968). "Gravity current and related phenomena." *J. Fluid Mech.*, 31(2), 209–248.

Bergant, A., Dudlik, A., Pothof, I., Schoenfeld, B. H., Tijsseling, A. S., and Vardy, A. E. (2005). "Case studies of inertia-driven fluid transients in pipe systems containing liquids." *Portuguese J. Water Res.*, 26(2), 37–44.

Bergant, A., Hou, Q., Keramat, A., and Tijsseling, A. S. (2011). "Experimental and numerical analysis of water hammer in a large-scale PVC pipeline apparatus." *Proc., 4th IAHR International Meeting on Cavitation and Dynamic Problems in Hydraulic Machinery and Systems*, Belgrade, Serbia, Univ. of Belgrade, October 2011, 27–36.

Bergant, A., and Simpson, A. R. (1999). "Pipeline column separation flow regimes." *J. Hydraul. Eng.*, 125(8), 835–848.

Bergant, A., Simpson, A. R., and Tijsseling, A. S. (2006). "Water-hammer with column separation: A historical review." *J. Fluid Struct.*, 22(1), 135–171.

Bergant, A., Tijsseling, A. S., Vítkovský, J. P., Covas, D. I. C., Simpson, A. R., and Lambert, M. F. (2008a). "Parameters affecting water-hammer wave attenuation, shape and timing. I: Mathematical tools." *IAHR J. Hydraul. Res.*, 46(3), 373–381.

Bergant, A., Tijsseling, A. S., Vítkovský, J. P., Covas, D. I. C., Simpson, A. R., and Lambert, M. F. (2008b). "Parameters affecting water-hammer wave attenuation, shape and timing. II: Case studies." *IAHR J. Hydraul. Res.*, 46(3), 382–391.

Bourdarias, C., and Gerbi, S. (2007). "A finite volume scheme for a model coupling free surface and pressurized flows in pipes." *J. Comput. Appl. Math.*, 209(1), 109–131.

Bozkus, Z., Baran, Ö. U., and Ger, M. (2004). "Experimental and numerical analysis of transient liquid slug motion in a voided line." *J. Press. Vessel Technol.*, 126(2), 241–249.

Bozkus, Z., and Wiggert, D. C. (1991). "Slug motion and impact in a voided line." *Proc., Fluid Transients and Fluid Structure Interaction, ASME Winter Annual Meeting*, ASME, New York, 25–27.

Bozkus, Z., and Wiggert, D. C. (1997). "Liquid slug motion in a voided line." *J. Fluid Struct.*, 11(8), 947–963.

Kayhan, B., and Bozkus, Z. (2011). "A mew method for prediction of the transient force generated by a liquid slug impact on an elbow of an initially voided line." *J. Press. Vessel Technol.*, 133(2), 021702-1–021702-12.

Koppel, T., and Ainola, L. (2006). "Identification of transition to turbulence in a highly accelerated start-up pipe flow." *J. Fluids Eng.*, 128(4), 680–686.

Laanearu, J., Bergant, A., Annus, I., Koppel, T., and van't Westende, J. (2009). "Some aspects of fluid elasticity related to filling and emptying of large-scale pipeline." *IAHR International Meeting of the Work Group on Cavitation and Dynamic Problems in Hydraulic Machinery and Systems*, Brno, Czech Republic, Brno Univ. of Technology, 465–474.

Laanearu, J., and van't Westende, J. (2010). "Hydraulic characteristics of test rig used in filling and emptying experiments of large-scale pipeline." *Proc., Hydralab III Joint User Meeting, Coastal Research Centre FZK of Leibniz Univ. and Technical Univ. Braunschweig*, Hannover, Germany, Leibniz Univ. and Technical Univ., Braunschweig, 5–8.

Leon, A. S., Ghidaoui, M. S., Schmidt, A. R., and Garcia, M. H. (2009). "Application of Godunov-type schemes to transient mixed flows." *IAHR J. Hydraul. Res.*, 47(2), 147–156.

Leon, A. S., Ghidaoui, M. S., Schmidt, A. R., and Garcia, M. H. (2010). "A robust two-equation model for transient-mixed flows." *IAHR J. Hydraul. Res.*, 48(1), 44–56.

Liou, C. P., and Hunt, W. A. (1996). "Filling of pipelines with undulating elevation profiles." *J. Hydraul. Eng.*, 122(10), 534–539.

Nydal, O. J., and Andreussi, P. (1991). "Gas entrainment in a long liquid slug advancing in a near horizontal pipe." *Int. J. Multiphase Flow.*, 17(2), 174–189, 0301-9322/91.

Politano, M., Odgaard, J., and Klecan, W. (2005). "Numerical simulation of hydraulic transients in drainage systems." *(MECOM—VIII Congreso Argentino de Mecanica Computacional) Mecanica Computacional (Argentina)*, Buenos Aires, Argentina, Mechánica Computacional, 297–310.

Vasconcelos, J. G., and Wright, S. J. (2007). "Comparison between the two-component pressure approach and current transient flow solvers." *IAHR J. Hydraul. Res.*, 45(2), 178–187.

Vasconcelos, J. G., Wright, S. J., and Roe, P. L. (2006). "Improved simulation of flow regime transition in sewers: Two-component pressure approach." *J. Hydraul. Eng.*, 132(6), 553–562.

Wylie, E. B., and Streeter, V. L. (1993). *Fluid transients in systems*, Prentice Hall, Englewood Cliffs, NJ.

Zhou, F., Hicks, F. E., and Steffler, P. M. (2002). "Transient flow in a rapidly filling horizontal pipe containing trapped air." *J. Hydraul. Eng.*, 128(6), 625–634.

Zukoski, E. E. (1966). "Influence of viscosity, surface tension, and inclination on motion of long bubbles in closed tubes." *J. Fluid Mech.*, 25(4), 821–837.

J. Hydraul. Eng. 2012.138:1090-1100.